Information Environment in JAIST

Teruo Matsuzawa, *Research Center for Advanced Computing Infrastructure (RCACI), Japan Advanced Institute of Science and Technology (JAIST)*

ABSTRACT: *The Research Center for Advanced Computing Infrastructure supports users' world-class research and educational environment by providing a high-speed advanced information environment. A high-speed, high-availability network provides the foundation for the high performance file servers, massively parallel computers, and various servers that have enabled JAIST since its foundation to continuously provide users a convenient information environment. I would like to introduce JAIST, the information environment in JAIST and our laboratory activities. We have continued to study for the Computational Fluid Dynamics (CFD) and HPC. Especially, biomechanics flow is major subject. In this paper, we are described four subjects that are Air-Flow Simulation in Nasal Cavity, Blood Flow Simulation in Thrombosed Aortic Dissection, Blood Flow Simulation in Aneurysm with STENT and Heart Simulation using Medical Images Voxel Based Fluid-Structure-Cell Interaction Analysis.*

KEYWORDS: Campus network, Massively Parallel Computers, Computational Fluid Dynamics (CFD), Bio-Fluid Mechanics, Image based Analysis, Nasal Cavity Flow, Ulcer-Like Projection (ULP), Stent, Heart Simulation, Voxel based Fluid-Structure-Cell Analysis

1. Introduction to Japan Advanced Institute of Science and Technology (JAIST)

JAIST was established in October, 1990 as Japan's first national graduate institute without undergraduate division that held an independent campus and programs of education and research to pursue world-class researches in advanced science and technology.

1.1 JAIST's Aims

JAIST aims at providing the highest level of education and research in the world and contributing to securing and enhancing Japan's status as a world leader in technology. To materialize such aims JAIST has developed leading researchers and engineers for industries as well as academic institutions.
Our Goals and methods are as following,

- To help students develop as excellent researchers and engineers who will serve the well-being of humankind, we offer a systematic educational program in an advanced academic environment.
- To promote organized research activities of the highest quality and create a world-class center of excellence, we contribute to society through active collaboration and cooperation with academia, government, and industry.
- To become an institution with a truly global perspective, we accept students and faculty members from abroad, and promote international joint research.

JAIST pursues

- Accumulation of outstanding scholarly achievements, based on organized research activities of the highest quality
- Systematic education program for future leaders who will serve the welfare of humankind
- Advanced education and research through active collaboration and cooperation among academia, government, and industry

1.2 Three Schools

JAIST offers only graduate programs and consists of three graduate schools, School of Knowledge Science, School of Information Science and School of Materials Science.

The School of Knowledge Science is the world's first research and education institute established under the theme of knowledge. We investigate knowledge formation and communication processes in organizations from the perspective of the social sciences, investigate group decision-making processes from the perspective of the cognitive sciences to establish information systems that support the creation of knowledge including groupware, and attempt to clarify the nature of knowledge through research on complex systems and genetic information. We approach various issues from the perspective of "knowledge," a new point of view, freely, employing every means possible without regard to the borders of the traditional disciplines. Although it is very clear that "knowledge" is an extremely important concept in considering the direction in which our society should move, we have not yet identified the important issues yet. For example: "What is knowledge?"; "Of what practical use is knowledge?"; or "How can knowledge be created?". Our approach is to seek the answer to such questions and consider our future with a focus on "knowledge."

The objective at the School of Information Science is to promote international-level cutting-edge research in Japan. The number of its staff and other factors make the School of Information Science at JAIST one of Japan's leading information science faculties and departments. The school, therefore, is well-positioned to cover a broad area of research. Moreover, one of the key features of the school since its establishment has been to focus on basic research in anticipation of developments in the field of information science. The school has 5 research and education regions as follows;

- Theoretical information science
- Human information processing
- Artificial intelligence
- Computer systems and networks
- Software science

The School of Materials Science comprises the fields of physics, chemistry, and biology – with activities covering a wide range of studies from theory to application in each of the fields of materials science. In the field of physics, for example, we are involved in the development of semiconductor devices and superconductive materials as well as the surface analysis in nano space. In the field of chemistry, we engage in organic materials chemistry, solid catalyst design, and the creation of nano particles and solutions with new functions. And in the field of biology, we are involved in the development of next-generation bio analysis devices and biomaterials. Since the establishment of the School of Materials Science, we have considered the integration of these three fields to be an essential requirement for the development of advanced science and technology.

1.3 About JAIST

We have academic exchange agreements with nearly 91 foreign academic or research institutes 26 foreign countries. In addition to world-class research collaborations and acceptance of talented international students, we are operating four dual degree programs in which participating students can obtain two graduate degrees at the same level from their home institute and JAIST. The students can take advantage of excellent opportunities in education and research offered by the two institutes. English is the language of instruction in every course at the Doctoral level and most of the courses at the Master's level. We take the 20th anniversary as the Beginning of the Second Period of Founding to further promote the advanced education and research activities so that JAIST will keep developing as a leading international graduate institute in the world.

2. Introduction to Information Environment at JAIST

2.1 Introduction

Addressing various needs from education and research of advanced science and technology area, Research Center for Advanced Computing Infrastructure (RCACI) builds, manages and provides the world class information and communication environment such as;

- High speed and highly-available network
- High performance and large scale storage
- Large scale & high performance MPC's
- Highly-secured environment

The RCACI has two groups; Operation group and Research and development (R&D) group. The missions of the former group are as follows;

- Providing well balanced and high level ICT service, and ongoing quality enhancement for Knowledge, Material and Information science education/research activities, library and administration sections
- Building and operating ICT system as a leader among ICT centers of Japan

- Contribution to world class network building

The second group develops challenging technology for supporting ICT based society, and provides vast demonstration experiments on technology.

- Next-generation complex ICT system (Cloud)
- Next-generation network for internet
- MPC system development for supporting education & research of advanced science and technology
- Security technology to realize the ease & safe ICT society

2.2 Networks

The bandwidth of backbone network is 10Gbps. The bandwidth of the other networks is 1Gbps. The wireless network is built over all campus including dormitory (Fig.1).

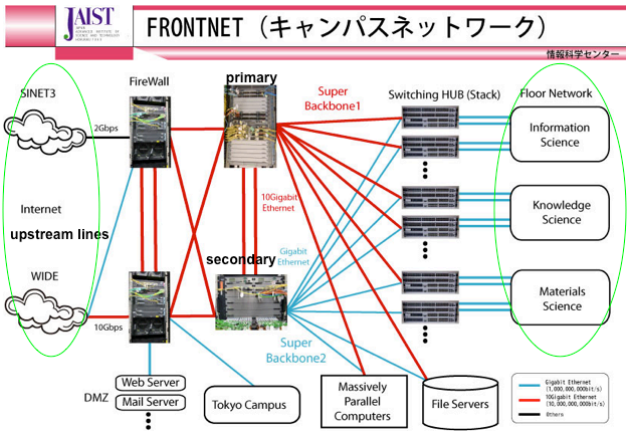

Fig.1 Campus network in JAIST (FRONTNET)

2.3 MPC systems

Fig.2 shows that there are 5 MPC systems in JAIST.

- Cray XT5: AMD Opteron 2048-cors, 4TB Memory, 19.6TFLPS
- SGI Altix 4700: Itanium2 192cores, 2.3TB Memory, 1.2TFLOPS
- DGI Altix XE Cluster: Xeon 40-cors/5-node, Zeon 8-cores & Altea Stratix IIIx 3/1-node
- NEC SX9: 4-cpu, 256GB Memory, 409.6GFLOPS
- Appro PC Cluster: Zeon 512-cors/64-node/1.5TB & 192-core/8-node/1TB
- IBM QS22: PowerX cell 8i 16-cpu/8-node/64GB Memory

2.4 Private Cloud System

The private cloud system is introduced at April 2010 in Fig.3. This system is built using VM ware and Citrix ZenApp.

Fig.2 Massively Parallel Systems in JAIST

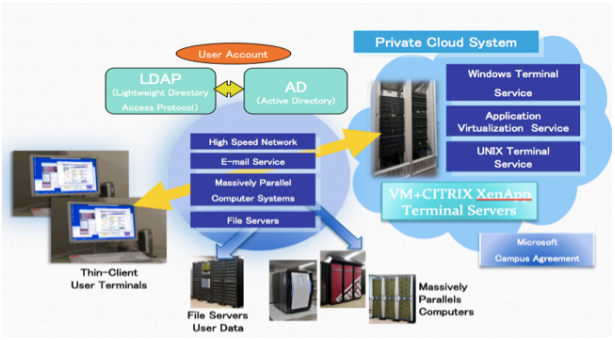

Fig.3 Private Cloud System in JAIST

3. Our Research Activities

3.1 Introduction

We have continued to study for the Computational Fluid Dynamics (CFD) and HPC. Especially, biomechanics flow is major subject. In this paper, we are described four subjects that are Air-Flow Simulation in Nasal Cavity, Blood Flow Simulation in Thrombosed Aortic Dissection, Blood Flow Simulation in Aneurysm with STENT and Heart Simulation using Medical Images Voxel Based Fluid-Structure-Cell Interaction Analysis.

3.2 Air-Flow Simulation in Nasal Cavity

3.2 .1 Introduction

The nasal cavity has complex anatomy, and the flow in nasal cavity is complex. The nasal cavity has functions that are breathing, smelling, humidification, warming and cleaning of the inhaled air. By these functions, humans can adapt to harsh environments. And, the nasal cavity has paranasal sinus that divides into four ports depend on

location, 1) Maxillary Sinus, 2) Forntal Sinus, 3) Ethmoidal Sinus, and 4)Sphenoid Sinus. Biomedical significant of paranasal sinus are humidification, resonance and lightening of the skull. But, physiological functions have not understood sufficiently. In this research, we focus on especially Maxillary sinus that is largest part in the paranasal sinus. Therefore, it is thought that maxillary sinus is most influential to main flow of nasal cavity. And, the model is using biological heat and humidity transfer from the organ side via membrane. We examine that flow and functions of in nasal cavity using numerical simulation by finite volume method [1] [2]. To clarify a function of nasal cavity, we calculate airflow of nasal cavity using heat and humidity model.

3.2.2 Method

The nasal cavity wall is composed of mucous membranes, blood vessel, and etc. The temperature and humidity of the inhaled air are adjusted by function of the mucous membranes. In this work, we focus on heat and humidity transfer from the organ side via membranes. Therefore, heat and humidity models are used that is developed by us [3]. Fig.4 shows that the geometry of nasal cavity includes maxillary sinus was reconstructed from medical images (CT images). The parameters of the CT images are around 50 years old Japanese male, resolution 512x512, pixel size 0.234[mm], and slice pitch is 0.3[mm]. The calculation conditions are temperatures of inflow are 0[ºC] and 25[ºC], humidity is 70 %, the wall was assigned human body temperature 34[ºC], and the velocity of inhaled air is 0.804[m/s].

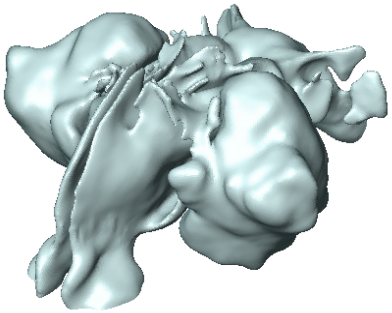

Fig.4 Reconstruction Shape of Nasal Cavity

3.2.3 Result

Fig.5 shows that airflow in nasal cavity is visualized by streamline. The high velocity area is middle meatus. And, superior meatus and inferior nasal meatus is low velocity area. In the maxillary sinus, airflow is quite slow in comparison with main flow of nasal cavity. And, flow patterns of left and right maxillary sinus are different. In addition, large swirling flow is seen in the each of maxillary sinus. Fig.6 shows the temperature distribution of nasal by contours. Fig. 6 (a) shows that temperature distribution that temperature of inhaled air is 0[ºC]. The inhaled air is heated by absorbing heat from the organ side via the membrane. Most Temperature change occurred in the front region of nasal cavity. And, Fig. 6 (a) indicates that the air temperature increased with increasing distance from the nares. Fig. 6 (b) shows the temperature distribution that temperature of inhaled air is 25[ºC]. The inhaled air became hot by heat supply from the organ side via the membrane. In this Fig. 6 (b) case, Most Temperature change also occurred in the front of nasal cavity. Temperature of inhaled air is heated to almost temperature of organ side at middle of nasal cavity.

Even if temperature is low at the nares such as Fig. 6 (a) case, inhaled air is heated to suitable temperature that is almost organ side temperature (34[ºC]) until it come at pharynx. In the maxillary sinus, temperature is kept high at the case that temperature of inhaled air is low.

Fig.7 shows the humidity distribution of nasal cavity by contours. Fig. 7 (a) shows humidity distribution that temperature of inhaled air is 0[ºC]. The inhaled air became humid by absorbing water from the organ side via the membrane. In addition, the inhaled air became increasingly humid with increasing distance from the nares. Most of change in the relative humidity also occurred in the front of nasal cavity. Fig.7 (b) shows the humidity distribution that temperature of inhaled air is 25[ºC]. The inhaled air is humidified by water supply from organ side via membrane. The humidity of inhaled air is increased with increasing distance from the nares. Humidity of inhaled air is humidified to suitable humidity that is organ side humidity (100%) until it came at pharynx. In the maxillary sinus, humidity is kept high.

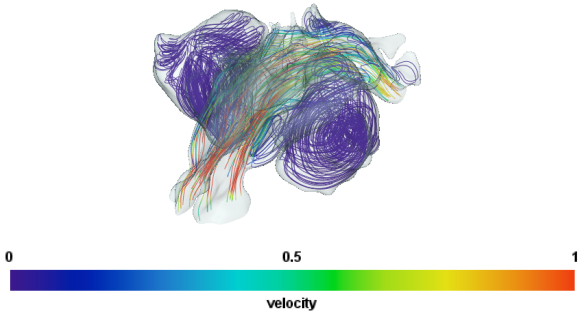

Fig.5 Airflow of Nasal Cavity

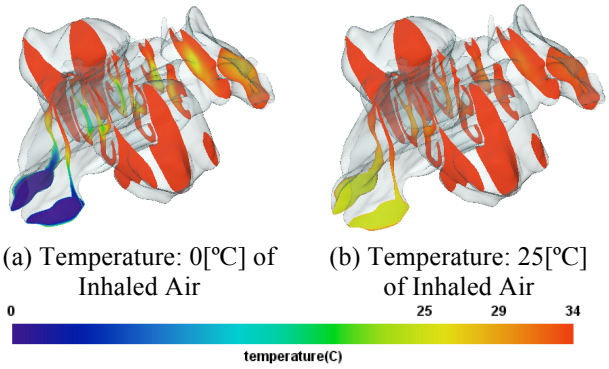

(a) Temperature: 0[ºC] of Inhaled Air

(b) Temperature: 25[ºC] of Inhaled Air

Fig.6 Temperature Distribution

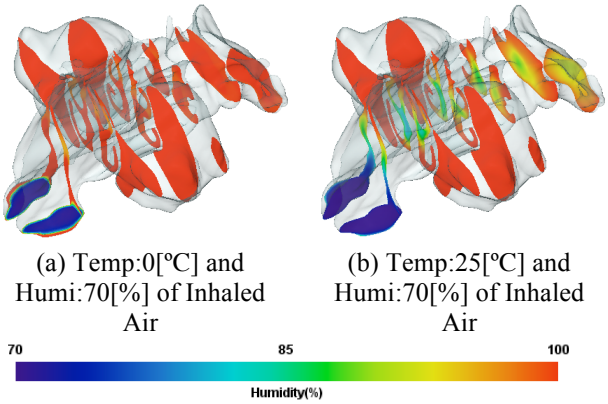

(a) Temp:0[ºC] and Humi:70[%] of Inhaled Air

(b) Temp:25[ºC] and Humi:70[%] of Inhaled Air

Fig. 7 Humidity Distribution

3.2.4 Summary

We examine the flow of nasal cavity include maxillary sinus. Temperature and Humidity of inhaled air are adapted to suitable condition by function of nasal cavity. In the maxillary sinus, temperature and humidity are maintained high and velocity of airflow is low. In addition vortex flow was seen in the each of maxillary sinus.

3.3 Blood Flow Simulation in Thrombosed Aortic Dissection

3.3.1Introduction

The pathogenesis of aortic dissection is an intimal tear or damage to the aortic wall. This condition is characterized by the rapid development of an intimal flap that separates the true lumen from the false lumen. Intimal flap tears are characteristic of communicating dissection. However, tears are not always identified and non-communicating dissections are not uncommon. These dissections can be classified on basis of blood flow in false lumen. Aortic dissections with patent proximal and patent distal re-entry tears in the absence a thrombus are defined as patent type. Dissections with a false lumen that is filled with thrombus and no longer communicates with the true lumen are defined as thrombosed type. The mean 3-year mortality rate for patients with a patent false lumen was found to be 13.7%, and for those with complete thrombosis was found to be 22.6% [4]. The mortality rate for the thrombosed type is higher than that for the patent type. In the thrombosed type, it has been reported that although the false lumen is completely occluded by the thrombosis, blood flow may be preserved, and the aneurysm may form. There is Ulcer-Like Projection (ULP) as a process to the aneurysm of the thrombosed type [5]. ULP is an ulcer part from intimal to false lumen and suggests entry part. In thrombosed type, ULP is frequently seen, however, it is not understood whether ULP is a time-dependent change. Therefore, a time-dependent change of ULP is important in diagnosis. The diagnosis of an aneurysm is required careful selection of a treatment. Currently, diagnosis by computed tomography (CT) is mainly used. CT can retrospectively reveal these changes by examination of a series of images. However, there have been no reports on predicting these life-threatening changes. Hence, only images are employed for diagnostic purposes. This places significant limits upon the diagnosis of this condition.

It has been established using a Computational Fluid Dynamics (CFD) simulation that dynamic stress is a risk factor for development, progression and rupture of an aneurysm. In contrast, the present study is designed to predict progression and rupture of an aneurysm using time series medical images obtained after development and immediately before rupture. Valuable information can be obtained by combining a clinical diagnosis and with the results of CFD calculations. The aim of this study is clarified the hemodynamics predictive factor. A dynamics stress as risk factor was related for progress and rupture of aneurysm due to the thrombosed dissected thoracic aorta.

3.3.2 Method

We were reconstructed the blood vessel from time-series medical images and were analysed. Fig.8 shows reconstruction shape in time-dependent change. We called as case1-A that is a certain state of ULP and case1-B that is before immediately rupture of ULP, respectively. The blood flow is simplified as the isothermal, incompressible Newtonian fluid, and laminar flow.

The blood density is ϱ=1050 kg/m^3; the dynamic viscosity of blood is μ=0.0035 Pa•s. The boundary conditions of the inlet, outlet, blood vessel, aneurysm wall, and stent are time-independent. The inlet boundary condition was uniform velocity profile with 0.6 [m/s]. Outlet boundary condition was set to corresponding to the distance from the inlet.

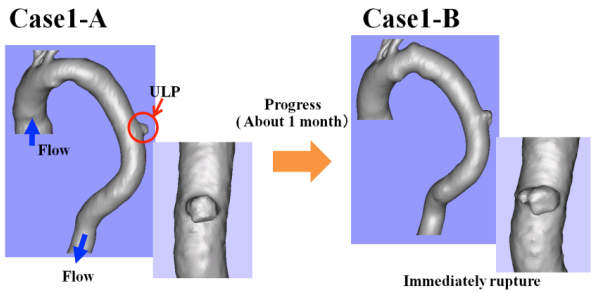

Fig.8 Reconstruction Shape of thrombosed aortic dissection from time-series medical image : Case1-A is a certain state of ULP due to thrombosed aortic dissection. In Case1-B, ULP is a state immediately before rupture.

3.3.3 Result

Fig.9 shows flow pattern. The high flow is seen in back, and the slow flow is seen in inside. Moreover, the vortex was observed at ULP. Inflow to ULP flows along the wall. To examine the flow aspect for the aneurysm, we observed the secondary flow around the aneurysm. The horizontal section slice decides an on the left, right, top and bottom based on the direction of the secondary flow in vertical section. Fig.10 shows a secondary flow in horizontal section based on vertical section. In each slice, we examine the vortex. The move of center of vortex agrees with direction of based on secondary flow in vertical section. Fig.11 and Fig.12 shows pressure and wall shear stress (WSS) distribution. This range is used to emphasize the ULP region. A region of high pressure distribution is seen below and edges the ULP. When observe the development case1-B, ULP is processing in part of high pressure distribution. Moreover, ULP in case1-B is uniform pressure distribution in whole. In case1-A, high WSS distribution is seen in top of ULP and low WSS distribution is seen in edge of ULP. When observe the development case1-B, ULP is processing in part of low WSS distribution. Similarly, low WSS distribution is seen at edge of ULP in case1-B. We thought that low WSS distribution progresses further. And low wall shear stress distribution tends to be seen in the direction where the vortex was moved.

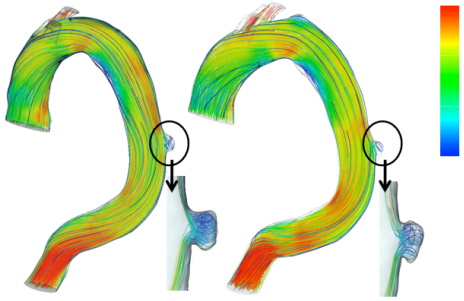

Fig.9 Flow Pattern in whole and close-up ULP

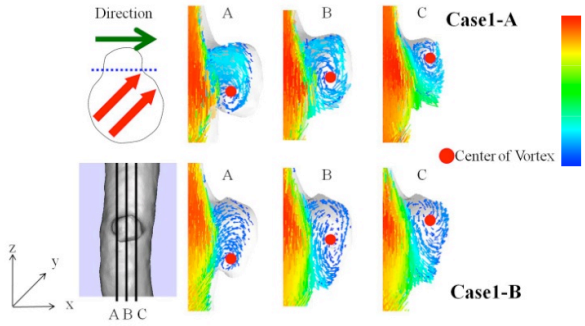

Fig.10 Secondary flows in horizontal section in ULP (upper) Case1-A (below) Case1-B: red point show center of vortex

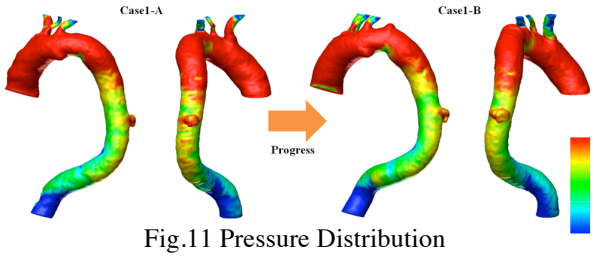

Fig.11 Pressure Distribution
(left) Case 1-A (right) Case1-B

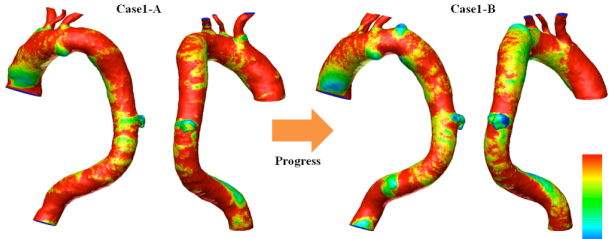

Fig.12 Wall Shear Stress Distribution
(left) Case 1-A (right) Case1-B

3.3.4 Summary

We examined the prediction of hemodynamic factor in the thrombosed aortic dissection. This investigation has indicated that a developing aneurysm occurs in region with high pressure distributions and low WSS region at entry part. This time-dependent of change is important the movement of center of the vortex in ULP.

3.4 Blood Flow Simulation in Aneurysm with Stent

3.4.1 Introduction

The cerebral aneurysms are pathologic dilations of the arterial wall that frequently occur near arterial bifurcations in the circle of Wills. The most serious consequence is their rupture and intracranial haemorrhage into the subarachnoid space, with an associated high mortality and morbidity rate. There are open surgery and clipping of aneurysm and endovascular treatment as treatment for cerebral aneurysm. Surgical treatment of

health costs is higher than that of endovascular treatment. Thus, endovascular treatment is paid attention as treatment of cerebral aneurysm. Endovascular treatment is a low invasive therapy and involves the development of platinum coils into the aneurysm. The objective of endovascular treatment is to shield the aneurismal wall and reduce the blood flow into aneurysm, thus progressively inducing aneurismal flow stasis, thrombus formation and aneurysm occlusion. Recently, the effect of only stent on the flow reduction in cerebral aneurysm has been reported in Computed Fluid Dynamics (CFD) [6]. Moreover, the comparable effect is also reported in experiment [7]. Some results suggested that the blood flow into aneurysm can reduce by only stent placement. When treating stent treatment, the diameter of stent is larger than that of blood vessel diameter. Thus the blood vessel has been slightly expanded by stent placement is expected. However, some research is not consider the expansion blood vessel by stent placement

In this research, we analyze that considered the expansion of blood vessel by stent placement using idealized shape. And we clarify the effect of blood vessel expansion for stent treatment.

3.4.2 Method

Currently, stent of various porosity and design is developed. We construct the zigzag stent that has 16 vertexes using Rhinoceros 2.0. Fig.13 shows the constructed stent. The cross-section of constructed stent is circle. Fig.14 shows that the geometry is an idealized aneurysm. The parent blood vessel is a straight pipe and the aneurysm is a sphere. The parent blood vessel was 4[mm], the length was 320 [mm], the diameter of aneurysm was 8[mm], and the aneurismal orifice was 6 [mm]. And the reconstructed intracranial stent was placed to cover aneurysm neck completely as the definition of stent treatment. To consider the blood expansion by stent placement, the blood vessel diameter has been increase by 5%, 10%. A tetrahedron numerical mesh was generated with tetrahedron using commercial software (Gambit 2.2.30). Then, mesh refinement was used at stent neighborhood; the size of mesh in stent neighborhood was finer than other part. We called as “not blood vessel expansion (BVE)” that is not considered blood expansion and “**% BVE” that is considered BVE by 5% and 10%.The blood flow is simplified as the isothermal, incompressible Newtonian fluid, and laminar flow. The blood density is ϱ=1050 kg/m^3; the dynamic viscosity of blood is μ=0.0035 Pa•s. The boundary conditions of the inlet, outlet, blood vessel, aneurysm wall, and stent are time-independent. The inlet boundary condition was uniform velocity profile with 0.200[m/s]. Outlet boundary condition was set to 0 [Pa]. The Reynolds number was 240. No-slip condition was employed on the blood vessel, aneurysm wall, and stent.

3.4.3 Result

Fig.15 shows the flow pattern in cross section of center and vertical. The inflow to aneurysm is on the inflow side of the orifice. The flow that stepped over stent and along the artery wall was seen. When compare not BVE and 10% BVE, the inflow to aneurysm of 10% BVE has more decrease than that of not BVE. Moreover, the flow velocity has decreased more than not BVE. Fig.16 shows the wall shear stress (WSS) distribution. The WSS distribution is decreased by stent placemen in aneurysm part. Moreover, expansion blood vessel with stent is more decrease than that of with stent. When compare not BVE and 10% BVE, mean WSS distribution value has been decrease by 42%.

3.4.4 Summary

We examine the effect of stent to compare not expansion to expansion by 10%. By consider the expansion blood vessel by stent placement, the velocity and WSS distribution has decrease than not expansion.

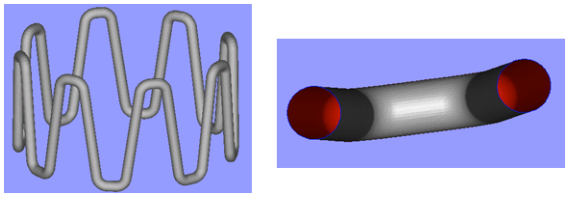

Fig.13 Idealized Stent Shape
(left) Whole (right) cross-section of stent

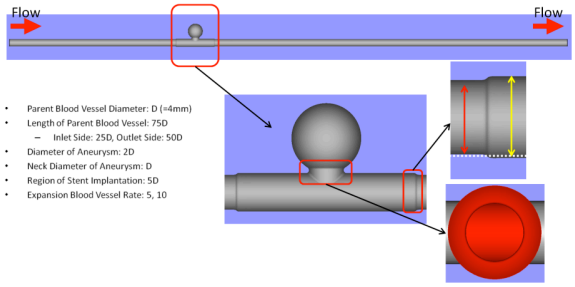

Fig.14 Idealized Blood Vessel Shape with Aneurysm

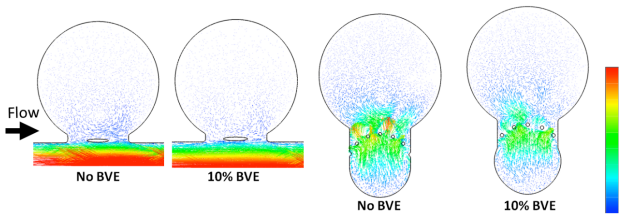

Fig.15 Cross Section View of Flow Pattern (left) Center (right) Vertical

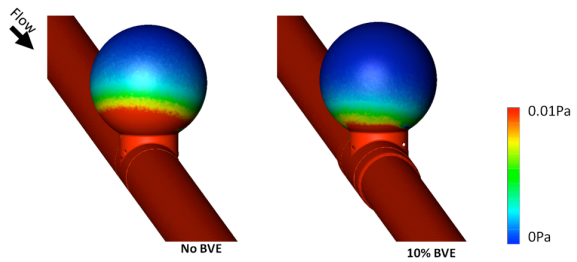

Fig.16 Wall Shear Stress Distribution (left) not expansion (right) expansion by 10%

3.5 Heart Simulation using Medical Images Voxel Based Fluid-Structure-Cell Interaction Analysis

3.5.1Introduction

Recently there are various computational fluid dynamics (CFD) approaches to know blood flow behavior in human body. Our aim is to perform realistic blood flow simulation considering with heart behavior using patient specific blood vessel and heart shape obtained by Computational Tomo-graphy (CT) images as voxel data to assist medical diagno-sis and treatment. The motion of heart wall driving the blood flow is occurred by cardiomyocyte contraction. And the cardiomyocyte behavior depends on the heart deforma-tion state. Therefore it needs to consider an interaction between cardiomyocyte behavior and heart deformation. To realize this interaction we have continued to develop the way for simulating the heart motion and the blood flow considering the cardiomyocyte behavior [8].

In this way, the cardiomyocyte behavior is simulated by the cell simulator "simBio" developed by "Cell/Biodynamics Simulation Project [9]" in Kyoto Univ. and cardiomyocyte model "Kyoto Model [10]" implemented on the "simBio". And to simulate the fluid-structure interac-tion between the heart wall motion and the blood flow, both calculated by same way to conventional CFD scheme. And using this system and left-ventricle model, we simu-lated heart wall deformation driven by cardiomyocyte contraction and blood flow.

3.5.2 Method

In general, the deformation of structure such as heart wall was calculated in Lagrangian frame that moves corres-ponding to the object deformation. But it is convenient to calculate the deformation in Eulerian frame because the human body data is obtained into voxel data by CT. To simulate heart motion in volume data, we have continued to develop the code for structure analysis in Eulerian frame.

By assumption blood and heart wall is incompressible continuum material, governing lows of incompressible continuum material are the mass conservation law and the momentum conservation low. Each described following equation (1) and (2). Equation (1) is called "equation of continuity" and it means the mass conservation law. Equa-tion (2) is called "Navier-Stokes equation" and it means the momentum conservation law.

$$\nabla \cdot \mathbf{v}_{mix} = 0 \tag{1}$$

$$\rho_{mix}\left\{\frac{\partial \mathbf{v}_{mix}}{\partial t} + (\mathbf{v}_{mix}\cdot\nabla)\boldsymbol{v}_{\mathbf{mix}}\right\} = -\nabla p + \nabla(\phi_f \boldsymbol{\sigma}'_f + \phi_s \boldsymbol{\sigma}'_s) \tag{2}$$

$\boldsymbol{v}_{mix}$ means the fluid flow velocity or the solid deformation velocity. ρ_{mix} means density of material, $\boldsymbol{\sigma}$ means stress tensor. Even though equations (1) and (2) are common governing equation of fluid and solid under incompressible condition, there is difference between fluid and solid in stress term. For fluid, by assuming that fluid is Newtonian fluid, $\boldsymbol{\sigma}'_f$ is fluid viscous stress shown in formula (3).

$$\boldsymbol{\sigma}'_f = 2\mu\mathbf{D} - p\mathbf{I} \tag{3}$$

Hence for the solid, by assuming that material is Neo-Hookean material of incompressible hyper-elastic material, $\boldsymbol{\sigma}'_s$ is solid deformation stress shows as following formula (4)[11].

$$\boldsymbol{\sigma}'_s = G\left\{\mathbf{B} - \frac{1}{3}\mathrm{tr}(\mathbf{B})\mathbf{I}\right\} \tag{4}$$

Here μ means viscosity, p means pressure, G means shear modulus. And I, B, D means unit tensor, Left Cauchy-Green deformation tensor, stretching tensor. Because stretching tensor D is described by velocity, the fluid viscous stress is able to define by velocity for the fluid. Hence for the solid, left Cauchy-Green deformation tensor B to define deformation stress is able to be calculated by solving advection equation (5) using velocity gradient tensor L.

$$\frac{\partial \mathbf{B}}{\partial t} + (\mathbf{v}_{mix}\cdot\nabla)\mathbf{B} - \mathbf{L}\cdot\mathbf{B} - \mathbf{B}\cdot\mathbf{L}^T = 0 \tag{5}$$

Because the solid stress that is defined by the strain natu-rally was defined by the velocity via the left Cauchy-Green deformation tensor, the solid deformation stress is also able to be solved by the same way to the fluid flow analysis.

In addition, to treat solid deformation, that is, the solid boundary moving in Eulerian frame, we employed VOF method [12]. In this method, volumetric ratio Φ of the solid is 0% in the cell having no solid and 100% in the cell filling by the solid. And volumetric ratio Φ of the solid is from 0% to 100% in the cell having the boundary between the fluid and the solid. The boundary moving is treated by advection of the volumetric ratio Φ. In Fig.17, green region means solid and white region means blank, and red arrow means deformation vector. After initial left state deforms, some cell have the boundary and each Φ value within from 0% to 100% in right state.

And to add the effect of the cardiomyocyte contractile force into the heart model wall deformation, we modified stress term as shown in formulations (6) to (8).

In those formulations, stress term is summation of the previously defined solid stress term (7) and the cardiomyocyte contractile force (8) calculated by the cell simulator "simBio" and cardiomyocyte model "Kyoto Model".

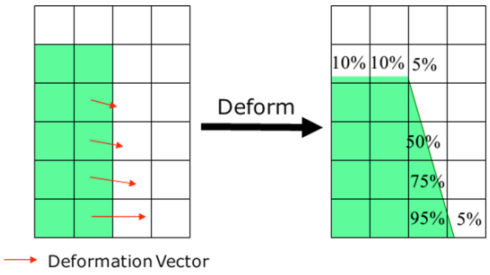

Fig.17 Advection of Volumetric Ratio Describing Deformation

$$\boldsymbol{\sigma}_s' = \boldsymbol{\sigma}_s^{Active} + \boldsymbol{\sigma}_s^{Passive} \quad (6)$$

$$\boldsymbol{\sigma}_s^{Passive} = G\left\{\mathbf{B} - \frac{1}{3}\mathrm{tr}(\mathbf{B})\mathbf{I}\right\} \quad (7)$$

$$\boldsymbol{\sigma}_s^{Active} = \text{Cardiomyocyte Contractile Force} \quad (8)$$

Cardiomyocytes have each own orientation in the heart wall. And the calculated contractile force was given as local contractile stress defined on the cardiomyocyte local coor-dinate system. To assign the local contractile stress into the global voxel data coordinate system, a coordinate transfor-mation for the contractile stress was performed by following way. First, the basis vectors e_i^O of the cardiomyocyte local coordinate system in the Cartesian system are made from the given cardiomyocyte orientation vector. Second, the rotation tensor R is made by e_i^O and the basis vector e_i^D of the global coordinate system.

$$\mathbf{R} = \mathbf{e}_i^O \otimes \mathbf{e}_i^D \quad (9)$$

Third, by rotation the cardiomyocyte local contractile stress σ_{Local} using the rotation tensor R, active stress σ_s^{Active} is obtained.

$$\boldsymbol{\sigma}_s^{Active} = \mathbf{R} \cdot \boldsymbol{\sigma}_{Local} \cdot \mathbf{R}^T \quad (10)$$

Orientation direction changes due to a deformation. Therefore the orientation basis vector change is tracked by solving this advection equation derived from Lagrange derivative.

$$\frac{\partial \mathbf{e}_i^O}{\partial t} + \left(\mathbf{v}_{mix} \cdot \nabla\right)\mathbf{e}_i^O = \mathbf{L} \cdot \mathbf{e}_i^O \quad (11)$$

For the verification of this orientation tracking scheme simple test was performed. In the test case, shearing veloci-ty, that cycle is 1.0 second, and initially vertical orientation vector were assigned in rectangle region. And track the orientation vector change. Resultant orientation vector moved to slant, and recovered corresponding to the velocity change. Exact solution of the angle and length are given by equation (12) and (13)

$$\theta_T = \mathrm{Tan}^{-1}\left(\frac{1-\cos(2\pi T)}{\pi}\right) \quad (12)$$

$$L_T = \frac{1}{\cos(\theta_T)} \quad (13)$$

Fig.18 show that comparing the angle and length with ex-act solution for 3 mesh divisioning 32x32, 64x64, 128x128. In both angle and length, numerical solution show good agree with exact solution for all mesh divisioning. From this result, our proposed tracking method can correctly track orientation change by deformation.

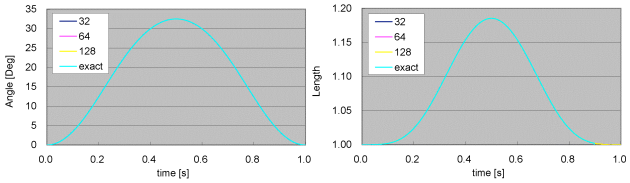

Fig.18 Comparing with Exact Solution (Left) Angle, (Right) Length

We discredited previously mentioned governing equation by finite difference method on staggered grid. For solving algo-rithm of this problem, we employed SMAC method that is familiar to simulate incompressible viscid flow as

shown in Fig.19. Here, in SMAC scheme algorithm, we replace viscous term in usual fluid calculation, into Neo-Hookean material stress term defined by velocity for velocity predictor calcu-lation. Unlike conventional SMAC method, the part to connect cardiomyocyte simulator SimBio and to update orientation vector e_i^o, volumetric ratio Φ, deformation tensor B are added in the algorithm.

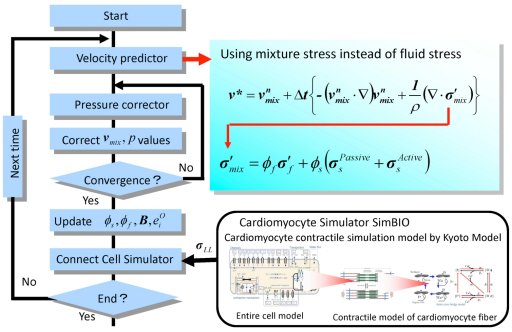

Fig.19 SMAC Scheme Algorithm

3.5.3 Numerical Experiment

Numerical experiment resembling to heart was performed. The test model was simple Left-Ventricle model and its motion driven by cardiomyocyte contractile was simulated. Model shape was half ellipsoid, short radius was 2.4[cm], long radius 3.6[cm], wall thickness was 1.0[cm]. Volume was 43[cm^3]. Inner fluid was 0.0035 [Pa•s] in viscosity and 1000[kg/m3] in density. Wall solid was 50k [Pa] in elasticity and 1050[kg/m^3] in density. Outer fluid was in 0.0035 [Pa•s] in viscosity and 1000[kg/m^3] in density. For this time, orientation vector was mixture of 2 kinds of direction component longitude and latitude. Shape and orientation component is shown in Fig.20.

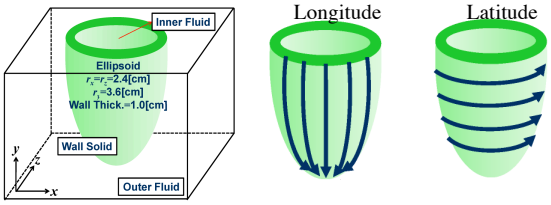

Fig.20 Test Case and 2 Orientation Components

For a boundary condition, on the upper plane that slices the ellipsoid, velocity was in free condition at the region of neighborhood of an inner fluid. And velocity was in non-slip condition at another region. On the all other plane velocity was in non-slip condition. A constraint condition for solid deformation was given by non-slip condition on the upper plane. The initial conditions of the orientation vector governing the direction of the contraction force were longitude-latitude ratio was 0%-100%, 25%-75%, 50%-50%, 75%-100% and 100%-0%. Fig.21 shows the ellipsoid shape at typical time for the longitude-latitude ratio was 50%-50% for orientation vector. The ellipsoid shrunk corresponding to the contractile force growing. At 0.1[s], it showed maximal shrink. After that, the ellipsoid recovered to the initial shape in proportion to the contractile force reduction. Red lines show that the ellipsoid recovered initial shape at 0.4[s]

Fig.22 shows the ejection fraction of several longitude ratio cases. Ejection fraction is ratio of difference between left-ventricle end diastolic volume and end systolic volume to the end diastolic volume. And it means how much blood the heart sends. After all, it is used as index of heart-pump function performance. This result shows that the orientation difference was cause of the difference of LV contractile magnitude. And the highest ejection fraction is found in case of the longitude 0% case, it value was about 40%. In actual heart, because end diastolic volume is 120[ml] and end systolic volume was 70[ml], ejection fraction is also about 40%. This result showed good agrees with actual heart.

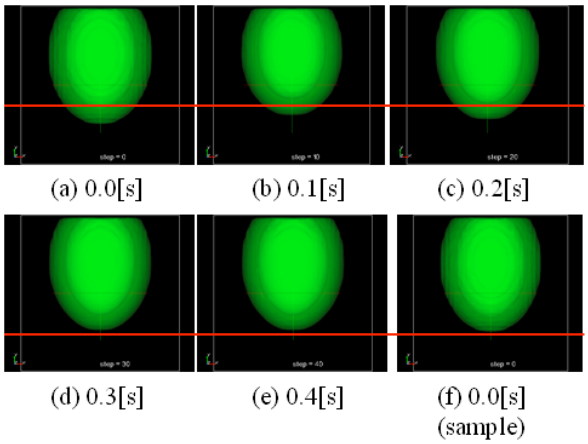

Fig.21 Shape at Typical Time

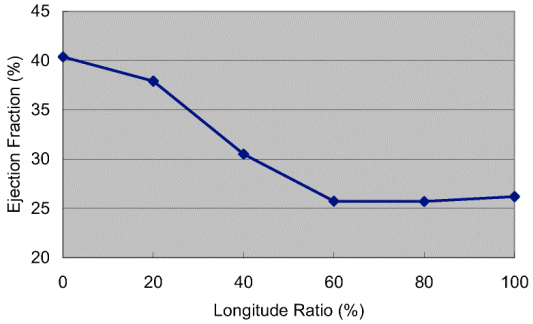

Fig.22 Ejection Fraction

3.5.4 Summary

To perform blood flow simulation driven by the heart wall motion considering the cardiomyocyte behavior using patient specific heart shape obtained by CT images as voxel data, we have developed the system considering the interaction between blood flow, heart wall deformation and cardiomyocyte behavior. In this system, blood flow and heart wall deformation are simulated by same way of SMAC method, which is very familiarized for CFD, by using constitutive equation of Neo-Hookean material described by velocity as a solid stress term of the momentum equation of incompressible continuum material. And we simulated heart model behavior using this scheme and obtained the result that the heart wall deformation is occurred by cardiomyocyte contractile force, and the blood flow is driven according as the heart wall deformation.

3.6 Our Research Activities Summary

We have paid lot attention about CFD and HPC. In this paper, we showed some our studies for biomechanics flow. And we continued to study these other subjects that are Hybrid parallelization for CFD software on multie-core cluster computer, Real-time visualization on distributed computing and New visualize scheme to emphasize complicated flow structure. We hope that computational biomechanics simulation will be a useful tool to improve medical and quality of life for everyone.

Acknowledge

In heart simulation study has been supported by "Next Generation Integrated Simulation of Living Matter" project in Japan [13]. And I really appreciate "Voxel branch, Organs/Whole Body-Scale Team (RIKEN, Tokyo Univ., Hiroshima Univ., Ritsumeikan Univ., Tokyo Univ. of Science, JAIST, et at al.) giving numerous amounts of advices. I express special thanks for my laboratory members.

Kiyoshi Kumahata (Now, Fujitsu Nagano Systems)
Fotoshi Mori (Ph.D. Student)
Shou Hanida (Ph. D. Student)

A part of this work is collaborated with Prof. Hiroshi Ohtake, Graduate School of Medical Science, Kanazawa University and Dr. Shigeru Ishikawa, Kanazawa Municipal Hospital.

Reference

[1] S.Ishikawa et al. Flow Mechanisms in the Human Olfactory Groove, Ach Otolaryngol Head Neck Surg, 135(2):156-162(2008).

[2] C.M.Hood et al. Computational modeling of flow and gas exchange in models of human maxillary sinus. Journal of Applied Physiology, 107:1195-1203(2009).

[3] K.Kumahata et al. Nasal Flow Simulation Using Heat and Humidity Models, Journal of Biomechanical Science and Engineering, 5(5):565-577(2010).

[4] T.Tsai et al. Partial thrombosis of the false lumen in patients with acute type B aortic dissection, New England Journal of Medicine, 357:349-359(2007).

[5] H.Hayashi et al. Penetrating atherosclerotic ulcer of the aorta: imaging features and disease concept, RadioGraphics, 20:995-1005(2000).

[6] G.R. Stuhne, D.A. Steinman. Mesh Resolution Requirements for the Numerical Simulation of Flow Through Stented Aneurysms, 2003 Summer Bioengineering Conference (2003)

[7] K. Baráth et al. Influence of Stent Properties on the Alteration of Cerebral Intra-aneurysmal Haemodynamics : Flow Quantification in Elastic Sidewall Aneurysm Models. Neurological Research, 27(1):120-128

[8] K. Kumahata et al. Fluid-Structure Interaction Simulation of the Heart driven by Myocardium Cell Behavior, Proceeding of The 4th Asian Pacific Conference on Biomechanics, 130-131 (2009).

[9] http://www.biosim.med.kyoto-u.ac.jp/

[10] N. Sarai et al. A Java package for the development of detailed cell models, Progress in Biophysics and Molecular Biology, 90:360-377 (2006).

[11]T. Hisada et al. Basis and Application of Non-linear Finite Element Method (in Japanese),Ma-ruzen: 65 (1995).

[12] C. W. Hirt, and B. D. Nichols. Volume of fluid (VOF) method for the dynamics of free boundaries. Journal of Computational Physics, 39: 201-225 (1981).

[13] http://www.csrp.riken.jp/index_e.html

About the Authors

Teruo Matsuzawa is a professor, Research Center for Advanced Computing Infrastructure (RCACI), Japan Advanced Institute of Science and Technology. He is a former Assistant to the president and former Director of Center of Information Science at JAIST. He can be reached at Research Center for Advance Computing Infrastructure, JAIST, 1-1 Asahidai, 921-8152 JAPAN. E-mail: matuzawa@jaist.ac.jp